JACS
JOURNAL OF THE AMERICAN CHEMICAL SOCIETY
Article
pubs.acs.org/JACS

Reversibility and Diffusion in Mandelythiamin Decarboxylation. Searching Dynamical Effects in Decarboxylation Reactions

Maite Roca,* Juan-Luis Pascual-Ahuir, and Iñaki Tuñón*

Departament de Química Física, Universitat de València, 46100 Burjassot, Spain

Supporting Information

ABSTRACT: Decarboxylation of mandelylthiamin in aqueous solution is analyzed by means of quantum mechanics/molecular mechanics simulations including solvent effects. The free energy profile for the decarboxylation reaction was traced, assuming equilibrium solvation, while reaction trajectories allowed us to incorporate nonequilibrium effects due to the solvent degrees of freedom as well as to evaluate the rate of the diffusion process in competition with the backward reaction. Our calculations that reproduce the experimental rate constant show that decarboxylation takes place with a non-negligible free energy barrier for the backward reaction and that diffusion of carbon dioxide is very fast compared to the chemical step. According to these findings catalysts would not act by preventing the backward reaction.

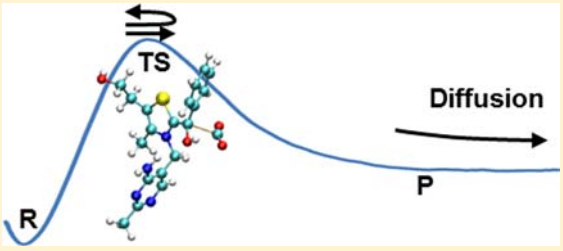

1. INTRODUCTION

Decarboxylation of 2-ketoacids is a primary metabolic process catalyzed by thiamin diphosphate-dependent enzymes.[1,2] This cofactor promotes decarboxylation through formation of covalent derivatives between the thiazolium moiety and the carbonyl group of the substrate. Mandelylthiamin (MTh, Scheme 1) is the conjugate of thiamin and benzoylformate,

Scheme 1

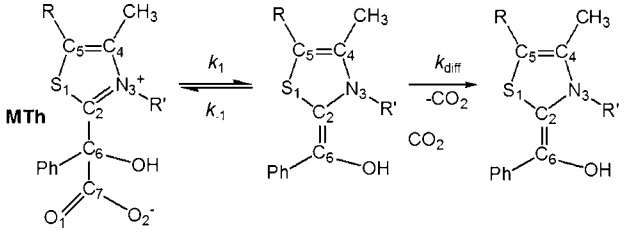

an analogue of the compound formed in the enzymatic decarboxylation of benzoylformate and a model to study the intrinsic reactivity of these enzymatic intermediates.[3−5] In aqueous solution MTh undergoes cleavage of a C−C bond resulting in the production of carbon dioxide with a rate constant (k_1 in Scheme 1) of 3×10^{-4} s^{-1} in neutral solution at 25 °C,[6] from which a phenomenological activation free energy of 22.3 kcal·mol^{-1} can be deduced applying standard transition state theory. This process is accelerated up to a factor of 4 in the presence of pyridinium ions but not by other Brønsted acids.[6] To explain these findings it was then proposed that in the absence of catalyst reversal addition of the enamine to carbon dioxide occurs readily (k_{-1} in Scheme 1) because they could be dynamically trapped in a solvent cage where the departure of carbon dioxide (k_{diff}) would be slow enough to allow recombination.[6−8] The catalyst would prevent the backward reaction in the solvent cage by protonation at C6 position prior to full diffusion of carbon dioxide,[8] being thus an example of the so-called spectator catalysis.[9]

However, recent quantum mechanical calculations with solvent continuum models showed that the backward reaction has a non-negligible free energy barrier, concluding that $k_{-1} \ll k_{diff}$.[10] Catalysis by pyridinium ions was then explained by means of preferential binding to the transition state due to a combination of cation/π and hydrogen-bonding interactions.[10] This elegant theoretical analysis is based on the following two premises: the validity of the equilibrium solvation picture and of the diffusional treatment of CO_2 motion just after bond breaking. With these assumptions this study showed that kinetic isotope effects (KIEs) observed for the $^{12}C/^{13}C$ substitution in carbon dioxide[7] can be reproduced only if decarboxylation and not the diffusion process is the rate-determining step.[10] The present work addresses directly the problem of reaction dynamics and products separation by means of molecular simulations explicitly accounting for the influence of the solvent degrees of freedom, including possible solvent-cage effects in the diffusion step. We will not only show that equilibrium solvation and free diffusional motion of the reaction products provide an appropriate framework for the treatment of MTh decarboxylation, but we will also discuss the limits of this approach in other decarboxylation reactions.

Received: March 19, 2012
Published: June 5, 2012

   dx.doi.org/10.1021/ja3026455 | J. Am. Chem. Soc. 2012, 134, 10509−10514

Dynamic effects can be incorporated to the rate-constant value derived from TST rate constant through the transmission coefficient (κ):[11−15]

$$k = \kappa \cdot k^{\mathrm{TST}} = \kappa \cdot \frac{k_{\mathrm{B}}T}{h}(C^0)^{1-n} \cdot \mathrm{e}^{-\Delta G^{\ddagger}/RT} \quad (1)$$

where $\Delta G^{\ddagger}$ is the activation free energy, n the number of reactant species, C^0 the concentration of the standard state (usually 1 M), T is the temperature, while the rest of symbols represent fundamental constants. The calculated transmission coefficient reflects the quality of the coordinate chosen to trace the free energy profile and thus of the dividing hypersurface defining the transition state (TS). For systems with a very high dimensionality, as the one considered here when water molecules are treated explicitly, it would be very complicated to find the optimal coordinate to obtain the free energy profile considering all the degrees of freedom of the system and then a distinguished reaction coordinate must be chosen. In this case the C6−C7 distance (see Scheme 1) provides a reasonable choice. Obviously water molecules must play a role in the reaction as far as the negative charge initially located on the carboxylate group must be transferred to the rest of the solute. Their influence on the reaction process can then be evaluated by means of trajectories starting at the putative TS ensemble.

In this contribution we present a detailed molecular picture of the MTh decarboxylation reaction in aqueous solution considering explicitly the solvent molecules, their equilibrium effects on the reaction free energy profile, and the dynamic influence on barrier recrossings and product diffusion. Moreover kinetic isotope effects (KIEs), which are frequently employed to deduce mechanistic details, are computed for the decarboxylation reaction in aqueous solution. Conclusions obtained from this work are of importance not only to understand the intrinsic reactivity of thiamin-derived compounds but also to analyze hypothetical catalytic strategies that could be employed by decarboxylases.[8]

2. METHODOLOGY

Our simulation model consists of mandelythiamin (MTh) substrate placed in a cubic box of pre-equilibrated water molecules (55.8 Å side) using the center of mass of the substrate as the geometrical center. Any water molecule with an oxygen atom lying in a radius of 2.8 Å from a heavy atom of the substrate was removed. Then the system contains 5802 water molecules and MTh (17457 atoms in total). The quantum mechanics (QM) region consists of MTh (51 atoms) and was treated by the semiempirical method AM1,[16] and the water molecules were described by means of the TIP3P potential[17] as implemented in fDynamo library.[18,19]

Initially the system was optimized and equilibrated by means of conjugate gradient optimization and molecular dynamics (MD) simulations. A switched cutoff, from 12 to 14 Å, was employed for all nonbonded interactions. MD simulations were performed at 298 K using the NVT ensemble and the Langevin−Verlet integrator with a time step of 1 fs. The total simulation time employed to equilibrate the system was 400 ps. All the quantum mechanics/molecular mechanics (QM/MM) calculations were carried out by applying periodic boundary conditions using fDynamo library.[18,19]

To analyze the energetics of the chemical reaction we performed the potential of mean force (PMF) at 298 K. The distance C6−C7 (see Scheme 1) was employed as a distinguished reaction coordinate. The umbrella sampling approach[20] was used to constrain the system close to a particular value of the reaction coordinate by means of the addition of a harmonic potential with a force constant of 2500 kJ·mol^{-1}·Å^{-2}. The probability distributions, obtained from a MD simulation within each individual window, are put together by means of the weighted histogram analysis method (WHAM)[21] to obtain the full probability distribution along the reaction coordinate.

Being aware that the semiempirical method AM1 does not always reproduce reaction barriers and reaction energies very well, we performed the PMF and subsequent analysis by applying a correction method that considers the inclusion of an interpolated correction energy term obtained as a function of the reaction coordinate:

$$E = E_{\mathrm{QM}}^{\mathrm{AM1}} + E_{\mathrm{QM/MM}}^{\mathrm{AM1}} + E_{\mathrm{MM}} + S\{E_{\mathrm{corr}}(D)\} \quad (2)$$

where the first term in the right-hand side of eq 2 is the energy of the QM subsystem, the second one is the interaction between the QM and MM subsystems, and the third is the energy of the MM subsystem. The last term is an interpolated correction obtained through a spline function (S) whose argument is the correction term.[22,23] The correction term is obtained as the difference between the energy provided by single-point energy gas phase calculations at a high level (HL) method and by a low level (LL) method for several configurations of the QM subsystem obtained along the chosen reaction coordinate. The LL energies were obtained using the AM1 Hamiltonian,[16] while the HL energies were obtained at the M06/6-31+G* level[24,25] of theory using *Gaussian09*.[26] The selected QM configurations were obtained along the AM1/MM minimum energy path traced down from the transition structure to the product and reactant valleys. A representation of this correction term as a function of the reaction coordinate is given in Figure 1. The selected DFT method provides a continuous correction energy in such a way that splines under tension can be used to interpolate the correction term at any value of the reaction coordinate. More details about this method are provided elsewhere.[22,23] We used this energy function (eq 2) in MD simulations to trace the PMF for the decarboxylation reaction as a function of the C6−C7 distance, from which the equilibrium activation free energy was derived. At this point it is worthy to point out that, while AM1 Hamiltonian has been shown to provide good energetic results for other decarboxylation reactions,[27] the large error observed in Figure 1 for MTh is partly due to the overestimation of the ionization energy of the enamine product, leading to too stable products. Vertical ionization energies for the enamine at various theoretical levels are given as Supporting Information (Table S1).

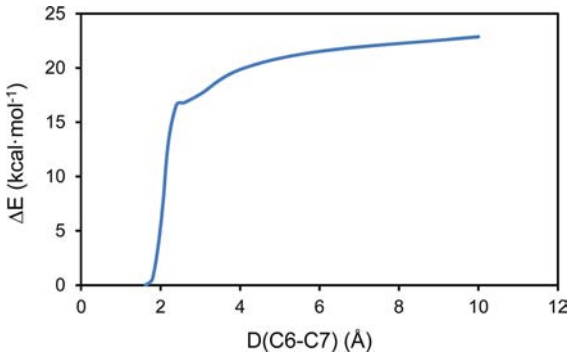

Figure 1. Correction energy term employed in the simulations of MTh decarboxylation. This was obtained as the single-point energy difference between AM1 and M06/6-31+G* calculations as a function of the C6−C7 bond length.

Once the PMF was obtained, we carried out 1 ns long QM/MM MD simulation with the system restrained to remain in the TS region using the same conditions as in the preceding simulations. One configuration was saved every 5 ps, resulting in 200 configurations that were used to compute free downhill trajectories. The velocity associated with the reaction coordinate is not properly thermalized in these configurations. Thus, following a procedure similar to that used by Gao and co-workers[28] and by us in previous studies,[29−31] we selectively removed the projection of the velocity on the reaction coordinate and added a random value taken from a Maxwell−

dx.doi.org/10.1021/ja3026455 | J. Am. Chem. Soc. 2012, 134, 10509−10514

Boltzmann distribution. For each of the saved configurations with modified velocities we ran free NVE simulations integrating the equations of motion forward and backward, just changing the sign of the velocity components. Downhill trajectories were propagated from −8 to +8 ps. The trajectories obtained were then classified as reactive trajectories when the reactants connect to products (RP trajectories), and nonreactive trajectories, where reactants connect to reactants or products to products. Both reactive and nonreactive trajectories may exhibit recrossings of the dividing surface. Because of the existence of recrossings, the transition state theory (TST) rate constant must be corrected by a transmission coefficient, κ, which will be less than unity. To compute κ we used the "positive flux" formulation,[32] by assuming that the trajectory was initiated at the barrier top with forward momentum along the reaction coordinate. For a given time, t (with t = 0 being the starting time for the downhill trajectory), the time-dependent transmission coefficient is defined as:

$$\kappa(t) = \frac{\langle j_+ \theta[q(+t)]\rangle - \langle j_+ \theta[q(-t)]\rangle}{\langle j_+ \rangle} \quad (3)$$

where q is the reaction coordinate, j_+ represents the initially positive flux at t = 0, given by $q(t = 0)$, and $\theta(q)$ is a step function equal to one in the product side of the reaction coordinate and zero on the reactant side. A correct evaluation of the transmission coefficient by means of this procedure obviously requires the convergence of the averaging procedure. This, in turn, will reflect the quality of the distinguished reaction coordinate and the selected TS ensemble. A poor choice would result in a too-small value of the transmission coefficient which would be very difficult to evaluate properly. We analyzed the changes in the environment as the reaction proceeds by means of detailed inspection of the reactive trajectories. In these analyses t = 0 indicates the passage of the system over the barrier top, negative times correspond to the evolution of the system toward the reactant valley, and positive times, toward the product one.

The rigid-rotor/harmonic-oscillator approximation was used with the CAMVIB/CAMISO programs[33−35] to calculate the KIEs for the $^{12}C/^{13}C$ substitution in carbon dioxide at 298 K. In order to obtain averaged values, from the 1 ns long QM/MM MD simulation with the system restrained to remain in the TS region, one configuration was taken every 100 ps, resulting in 10 TS structures. On the other hand, we also carried out 1 ns long QM/MM MD simulation with the system at the reactant-state region, and 10 reactant-state stuctures were saved. For each structure, we performed QM/MM relaxation of the geometry to either a local minimum or saddle-point, and at each stationary structure we computed the QM/MM Hessian in the presence of the environment effect using the core subset of atoms equivalent to the QM region (MTh, 51 atoms). The QM region was described by the M06/6-31+G* method for the QM/MM localization and characterization of the stationary structures. In order to perform DFT/MM calculations we used a combination of *Dynamo/Gaussian09* programs.[26,36,37]

3. RESULTS AND DISCUSSION

Figure 2 shows the free energy profile obtained for the decarboxylation reaction as a function of the C6−C7 distance. The activation free energy, corrected for the zero-point energy contribution (−1.8 kcal·mol^{-1}), is 22.1 kcal·mol^{-1}, close to the value derived from the experimental rate constant. For the reverse reaction we found that the equilibrium process is not barrierless. According to our simulations the free energy barrier for the attack of carbon dioxide on the enamine from the free energy plateau found at D(C6−C7) = 4 Å is 16.4 kcal·mol^{-1}, including a zero-point energy contribution of 1.2 kcal·mol^{-1}. Obviously, the barrier for the backward reaction is reduced, and the rate constant increased if we consider the carbon dioxide and the enamine in closer contact as the starting point of the reaction, but our equilibrium simulations did not show any free energy minimum or plateau at distances smaller than 3−4 Å.

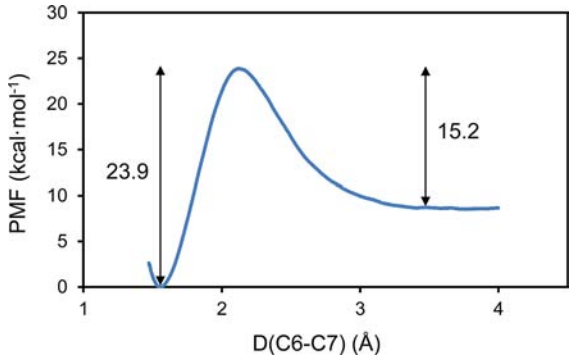

Figure 2. Potential of mean force for the decarboxylation of MTh.

In addition to the agreement with the experimental data, we confirmed the quality of our energy function (eq 2) comparing the results obtained with the set of 10 different TS structures located at the M06/MM level (see the Methodology section). First, the averaged C6−C7 distance for these M06/MM TS structures is 2.15 ± 0.06 Å, in excellent agreement with the position of the maximum of the PMF (2.14 Å). Second, for the M06/MM energy barriers determined after tracing the minimum energy reaction paths, we observed that the mean unsigned error provided by our energy function was 2.6 kcal·mol^{-1}, while the error at the AM1/MM level was 12.4 kcal·mol^{-1}.

After obtaining the PMF we investigated dynamical effects of the solvent on the reaction process to elucidate if solvent molecules could trap the reaction fragments at contact distances during a significant fraction of time. The rare-event simulations carried out from the transition state in the forward and backward directions were used to quantify barrier recrossings through the calculation of the transmission coefficient. This was obtained by means of the 'reactive flux formulation' (eq 3).[32] As seen in Figure 3, 65 fs after the

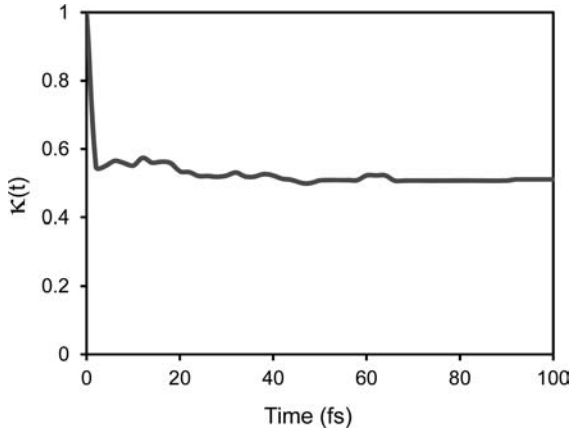

Figure 3. Time evolution of the transmission coefficient for the decarboxylation reaction of MTh. Time defines the evolution of the reaction passing through the transition state at t = 0.

passage over the top of the barrier, the transmission coefficient arrives to a plateau value of 0.51, which means that the fate of the reaction is completely determined after this period and no backward trajectories are observed afterward. The standard deviation of the measured transmission coefficient is 0.04, showing the convergence of the average over the set of trajectories. Deviation of the transmission coefficient from unity

dx.doi.org/10.1021/ja3026455 | J. Am. Chem. Soc. 2012, 134, 10509−10514

is an indication of solvent influence on reaction dynamics. It must be stressed that the transmission coefficient can be translated into an increase of the free energy barrier of only 0.4 kcal·mol^{-1} (at 298 K). Thus, the equilibrium picture, based on the use of the C6−C7 distance as the reaction coordinate, provides a reasonable estimation of the free energy profile and the free energy barrier, although the rate constants would be overestimated by a factor of ∼2. Using eq 1 we can now provide our best estimate of k_1 and k_{-1} rate constants, which are 2×10^{-4} and 3 s^{-1} respectively,[38] in excellent agreement with the experimental estimation of k_1.

The information obtained from the time-evolution of the transmission coefficient can be combined with the atomistic description obtained from the reactive trajectories presented in Figure 4 to have a more detailed view of the reaction process.

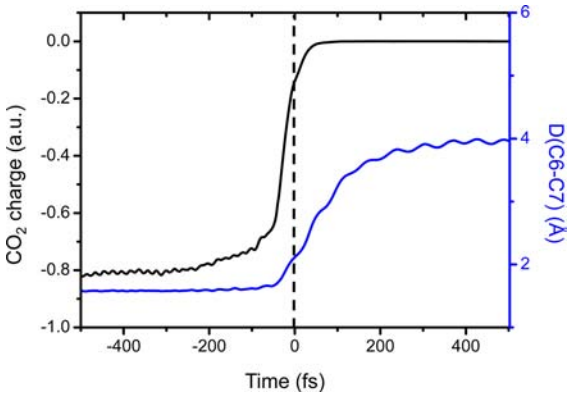

Figure 4. Averaged time evolution of the C6−C7 distance (blue) and the charge on the CO_2 leaving group (black) along reactive trajectories.

The average evolution of the C6−C7 distance and the total charge on carbon dioxide are plotted versus the reaction time. In this plot $t = 0$ (where t designates time) corresponds to the passage over the transition state from negative times (reactant state) to positive times (product state). It is interesting to note that at $t = 65$ fs, during which no backward trajectories were observed, the C6−C7 distance is about 2.8 Å. Thus, even at close contact distances between the carbon dioxide and enamine, the reaction to reformulate MTh from the product fragments is not a fast or barrierless process (see Figure 2). The free energy barrier is large enough to prevent any solvent effect favoring the reverse process.

During the reaction process, the charge on the CO_2 moiety must change from −1 au at the reactant state to zero at the product state. Such a variation is observed in Figure 4, but interestingly, the changes begin at $t \approx -300$ fs, significantly before the changes observed for the C6−C7 distance. This earlier variation in the charge is due to the rearrangement of the solvation shell of the two oxygen atoms of the carboxylate group which in turn polarizes the solute. The bond-breaking process can proceed only when CO_2 has already been partially desolvated and the charge has partially migrated to the enamine fragment. Figure 5 presents the time evolution of the electrostatic potential created by the solvent molecules on the oxygen atoms of the carboxylate group. Desolvation of this group is here reflected in the diminution of the potential created by the solvent. At the reactant state the potential is positive, as expected for a reaction field around a negatively charged group. Water molecules in equilibrium with the

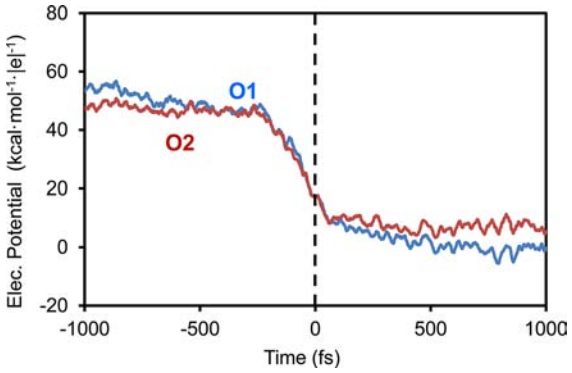

Figure 5. Averaged time evolution of the electrostatic potential created by the solvent on the oxygen atoms of the carboxylate group along reactive trajectories. Note that the changes begin significantly before to the passage of the system over the TS ($t = 0$).

carboxylate group are oriented in such a way that stabilizes the negative charge. In the product state, where the CO_2 is neutral, this potential is almost zero. It can be clearly observed that the variation in the electrostatic potential (this is in the arrangement of water molecules around the carboxylate group) clearly starts well before the passage of the system over the TS. The slower rotational and translational motions of water molecules must then precede the stretching along the reaction coordinate. This solvent participation in the reaction process is the origin of the recrossings observed in Figure 3.

We finally monitored the diffusion of the formed carbon dioxide by means of the time evolution of the average distances between the centers of mass of the two reaction fragments. Figure 6 plots this distance versus the square root of time, being

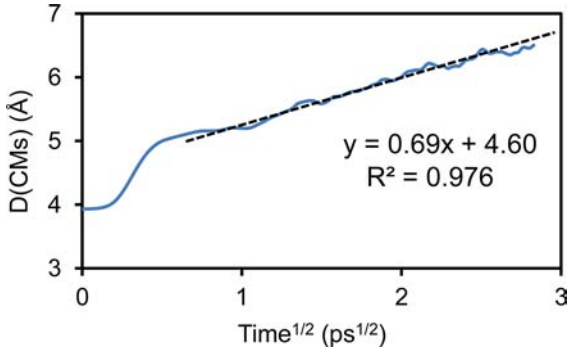

Figure 6. Averaged evolution of the distance between the centers of mass of carbon dioxide and enamine versus the square root of time. The results of the linear least-squares regression for $t > 1$ ps are also shown.

$t = 0$, the passage over the barrier top. It can be observed that the distance increases continuously without any evidence of formation of a stable solvent-trapped product complex. Figure 6 shows that for small times the relative motion of carbon dioxide and enamine is governed by chemical forces, but for $t > 1$ ps the distance between the centers of mass is a linear function of $t^{1/2}$, as predicted by the Einsteinian diffusion theory,[39]; thus, the motion is essentially due to collisions with solvent molecules. From the linear dependence between the distance and the square root of time (see Figure 6) we derived a diffusion coefficient for the relative motion of the two fragments (that corresponds to the sum of the diffusion coefficients of the two fragments, D_A+D_B) of 0.8×10^{-9} m^2·s^{-1}, similar to the

dx.doi.org/10.1021/ja3026455 | J. Am. Chem. Soc. 2012, 134, 10509−10514

experimentally determined diffusion coefficient of carbon dioxide in water, 1.9×10^{-9} $m^2 \cdot s^{-1}$.[40] We then estimated the rate constant for the diffusion process shown in Scheme 1 (k_{diff}) evaluating the time needed to separate the reaction fragments by diffusional motion up to a distance in which at least one water molecule could be placed between the carbon dioxide and the enamine, this is to separate them by ~3 Å more after the bond-breaking process. This disposition should be enough to prevent any fast rearrangement of the reaction fragments leading to the backward process. Using the derived diffusion coefficient we estimated that the lifetime of the product complex at contact distances would be of ~20 ps and then $k_{diff} \approx 5 \times 10^{10}$ s^{-1}. Otherwise, considering that carbon dioxide is uncharged, the diffusion rate constant for the product complex can be also be evaluated as:[41]

$$k_{diff} = 3\frac{D_A + D_B}{R^2} \tag{4}$$

where R is the contact distance between carbon dioxide and the enamine (when the diffusion process starts), which according to Figure 6 can be estimated to be ~5 Å. Then using eq 4 we obtained a value for $k_{diff} \approx 10^{10}$ s^{-1}, in good agreement with the previous estimation considering the approximations employed. In any case, the relevant point here is that any of the values obtained for k_{diff} are much larger than the rate constants estimated for the chemical steps, k_1 and k_{-1}.

In order to confirm that the chemical step is completely rate-detemining for the decarboxylation reaction, we have also calculated the KIEs observed for the $^{12}C/^{13}C$ substitution in carbon dioxide at the M06/MM level. We optimized 10 different TS and reactants structures (coordinates provided as Supporting Information, Table S2). From these structures, and assuming that the rate of the reaction is exclusively determined by k_1, we obtained an averaged estimation of the KIE of 1.056 ± 0.002 (see Supporting Information Table S3), in excellent agreement with the experimental estimation (1.058 ± 0.0005)[7] and with a previous theoretical estimations based on M06-2X calculations using a continuum solvent model (1.058).[10] The agreement obtained between different theoretical approaches (different functionals and different descriptions of the solvent) and the experimental value confirms that most probably the chemical step controls the rate of the global decarboxylation process.

Implications for Other Decarboxylation Reactions. Once it was seen that Einstenian law reasonably predicts diffusion of CO_2 just after bond breaking and given the value of the diffusion coefficient of this molecule in aqueous solution, we can speculate that the diffusion rate constant would be always around 10^{10} s^{-1} for this kind of reaction at room temperature. Then, the only way in which diffusion could be at least partly rate limiting would be in the case in which k_{-1} becomes of a similar order of magnitude. This would require an activation free energy for the backward process of about 3.8 kcal·mol^{-1}, a value considerably smaller than that predicted for the enamine recombination with carbon dioxide. Interestingly, a barrier of only 6.7 kcal·mol^{-1} has been theoretically obtained for the backward process of the orotate decarboxylation reaction.[27] In this case, diffusion would be about 10^2–10^3 times faster than the recombination process.

It must be noted that a free energy profile displaying a lower barrier for the reverse process may also imply a low-frequency TS. In such a case deviations from the equilibrium description of solvation effects can be more important, and smaller transmission coefficients could be observed. We can discuss these effects using Grote–Hynes (GH) theory to calculate the transmission coefficient as the ratio between the reactive frequency (ω_r) and the equilibrium barrier frequency (ω_{eq})[42,43]

$$\kappa_{GH} = \frac{\omega_r}{\omega_{eq}} \tag{5}$$

with the reactive frequency ω_r obtained via the GH equation:

$$\omega_r^2 - \omega_{eq}^2 + \omega_r \int_0^\infty \zeta_{TS}(t)\, e^{-\omega_r t}\, dt = 0 \tag{6}$$

where $\zeta_{TS}(t)$ is the friction kernel evaluated from the fluctuating forces acting on the reaction coordinate at the TS.[44] The equilibrium frequency for MTh decarboxylation (590 cm^{-1}) was derived from the PMF presented in Figure 2, while the transition state friction kernel was obtained from a 100 ps MD simulation carried out at the top of the PMF. The resulting friction kernel is given as Supporting Information (Figure S1). For MTh decarboxylation this theory predicts a transmission coefficient of 0.60 ± 0.04, in very good agreement with the value derived from MD trajectories. Interestingly, GH theory predicts that, for a constant friction kernel, the transmission coefficient diminishes when the equilibrium frequency diminishes (this is when the TS region becomes broader). By using eq 6 it is possible to discuss in which cases the transmission coefficient would be significantly smaller than unity, showing then a significant departure from the equilibrium picture. Figure 7 shows the evolution of the GH transmission coefficient with the equilibrium frequency. Transmission coefficients below 0.1 are expected for equilibrium frequencies below 300 cm^{-1}. Then, the use of activation free energies based on equilibrium solvation may lead to a significant overestimation of the rate constant for decarboxylation reactions with small equilibrium frequencies. In these processes participation of the solvent degrees of freedom in the reaction coordinate should be explicitly considered.

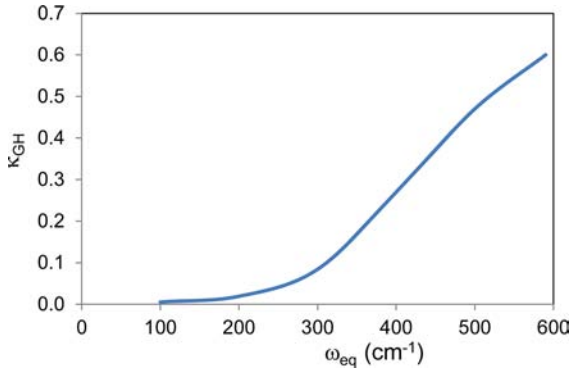

Figure 7. Evolution of GH transmission coefficient with the equilibrium frequency assuming a constant friction kernel obtained from simulations of MTH decarboxylation.

4. CONCLUSIONS

According to our molecular simulations of the decarboxylation reaction of MTh the chemical step and not the diffusion of the reaction products is the rate-limiting step even if dynamical solvent effects are included. Our estimation of the reaction constant of the forward reaction is in excellent agreement with the experimental value, while the values derived for the

dx.doi.org/10.1021/ja3026455 | J. Am. Chem. Soc. 2012, 134, 10509–10514

backward and diffusion processes show that the reaction products cannot overwhelmingly revert to the reactant valley but instead diffuse rapidly into the solution following Einstein law once chemical bonding forces are no longer in action. Our simulations show that: (i) diffusion could play a relevant role in decarboxylation kinetics only for those cases where the backward reaction presents a very low reaction barrier and (ii) important deviations with respect to the equilibrium solvation regime are expected for decarboxylations with low frequency barriers. MTh decarboxylation does not belong to either of these two categories.

According to the picture obtained, catalysis of MTh decarboxylation must not be attributed to protonation of the product complex prior to diffusion but rather to the preferential stabilization of the TS, as already shown in previous theoretical calculations.[10] The same conclusion about the origin of catalysis was reached in the case of histidine decarboxylation catalyzed by histidine decarboxylase, a PLP-dependent enzyme.[45] Studies on the decarboxylation process in thiamin diphosphate-dependent enzymes are currently in progress.

■ ASSOCIATED CONTENT

Supporting Information

Complete reference 26; vertical ionization energies of the product of MTh decarboxylation, coordinates of the QM subsystem for the TS and reactant structures located at the M06/MM level; individual estimations of KIEs; and a spectrum of the friction kernel. This material is available free of charge via the Internet at http://pubs.acs.org

■ AUTHOR INFORMATION

Corresponding Author

m.teresa.roca@uv.es (M.R.); ignacio.tunon@uv.es (I.T.)

Notes

The authors declare no competing financial interest.

■ ACKNOWLEDGMENTS

We gratefully acknowledge financial support from MICINN through project CTQ2009-14541-C02, from Generalitat Valenciana Projects ACOMP/2011/028, ACOMP/2012/243 and GV/2012/053 and from Universitat de València Project UV-INV-AE11-40931. M.R. thanks Ministerio Ciencia e Innovación for a 'Juan de la Cierva' contract. We acknowledge computational facilities of the Servei d'Informàtica de la Universitat de València in the 'Tirant' supercomputer. Authors acknowledge D. Laage for many helpful comments and the warm hospitality during the sabbatical stay of I. T. at the École Normale Supérieure (Paris).

■ REFERENCES

(1) Breslow, R. *J. Am. Chem. Soc.* **1957**, *79*, 1762.
(2) Breslow, R. *Chem. Ind.* **1957**, 893.
(3) Hu, Q. Y.; Kluger, R. *J. Am. Chem. Soc.* **2002**, *124*, 14858.
(4) Kluger, R.; Tittmann, K. *Chem. Rev.* **2008**, *108*, 1797.
(5) Polovnikova, E. S.; McLeish, M. J.; Sergienko, E. A.; Burgner, J. T.; Anderson, N. L.; Bera, A. K.; Jordan, F.; Kenyon, G. L.; Hasson, M. S. *Biochemistry* **2003**, *42*, 1820.
(6) Kluger, R.; Ikeda, G.; Hu, Q. Y.; Cao, P. P.; Drewry, J. *J. Am. Chem. Soc.* **2006**, *128*, 15856.
(7) Mundle, S. O. C.; Rathgeber, S.; Lacrampe-Couloume, G.; Lollar, B. S.; Kluger, R. *J. Am. Chem. Soc.* **2009**, *131*, 11638.
(8) Hu, Q. Y.; Kluger, R. *J. Am. Chem. Soc.* **2005**, *127*, 12242.
(9) Venkatasubban, K. S.; Schowen, R. L. *J. Org. Chem.* **1984**, *49*, 653.
(10) Gonzalez-James, O. M.; Singleton, D. A. *J. Am. Chem. Soc.* **2010**, *132*, 6896.
(11) Gertner, B. J.; Bergsma, J. P.; Wilson, K. R.; Lee, S. Y.; Hynes, J. T. *J. Chem. Phys.* **1987**, *86*, 1377.
(12) Alhambra, C.; Corchado, J.; Sanchez, M. L.; Garcia-Viloca, M.; Gao, J.; Truhlar, D. G. *J. Phys. Chem. B* **2001**, *105*, 11326.
(13) Poulsen, T. D.; Garcia-Viloca, M.; Gao, J. L.; Truhlar, D. G. *J. Phys. Chem. B* **2003**, *107*, 9567.
(14) Roca, M.; Moliner, V.; Tuñón, I.; Hynes, J. T. *J. Am. Chem. Soc.* **2006**, *128*, 6186.
(15) Olsson, M. H. M.; Parson, W. W.; Warshel, A. *Chem. Rev.* **2006**, *106*, 1737.
(16) Dewar, M. J. S.; Zoebisch, E. G.; Healy, E. F.; Stewart, J. J. P. *J. Am. Chem. Soc.* **1985**, *107*, 3902.
(17) Jorgensen, W. L.; Chandrasekhar, J.; Madura, J. D.; Impey, R. W.; Klein, M. L. *J. Chem. Phys.* **1983**, *79*, 926.
(18) Field, M. J. *A Practical Introduction to the Simulation of Molecular Systems*, 1st ed.; Cambridge University Press: Cambridge, U.K., 1999.
(19) Field, M. J.; Albe, M.; Bret, C.; Proust-De Martin, F.; Thomas, A. *J. Comput. Chem.* **2000**, *21*, 1088.
(20) Torrie, G. M.; Valleau, J. P. *J. Comput. Phys.* **1977**, *23*, 187.
(21) Kumar, S.; Bouzida, D.; Swendsen, R. H.; Kollman, P. A.; Rosenberg, J. M. *J. Comput. Chem.* **1992**, *13*, 1011.
(22) Ruiz-Pernia, J. J.; Silla, E.; Tuñón, I.; Marti, S.; Moliner, V. *J. Phys. Chem. B* **2004**, *108*, 8427.
(23) Ruiz-Pernia, J. J.; Silla, E.; Tuñón, I.; Marti, S. *J. Phys. Chem. B* **2006**, *110*, 17663.
(24) Zhao, Y.; Truhlar, D. G. *Theor. Chem. Acc.* **2008**, *120*, 215.
(25) Zhao, Y.; Truhlar, D. G. *Acc. Chem. Res.* **2008**, *41*, 157.
(26) Frisch, M. J.; et al.Gaussian, Inc.: Wallingford CT, 2009.
(27) Wu, N.; Mo, Y. R.; Gao, J. L.; Pai, E. F. *Proc. Natl. Acad. Sci. U.S.A.* **2000**, *97*, 2017.
(28) Nam, K.; Prat-Resina, X.; Garcia-Viloca, M.; Devi-Kesavan, L. S.; Gao, J. L. *J. Am. Chem. Soc.* **2004**, *126*, 1369.
(29) Roca, M.; Oliva, M.; Castillo, R.; Moliner, V.; Tuñón, I. *Chem.—Eur. J* **2010**, *16*, 11399.
(30) Ruiz-Pernia, J. J.; Tuñón, I.; Moliner, V.; Hynes, J. T.; Roca, M. *J. Am. Chem. Soc.* **2008**, *130*, 7477.
(31) Kanaan, N.; Roca, M.; Tuñón, I.; Marti, S.; Moliner, V. *Phys. Chem. Chem. Phys.* **2010**, *12*, 11657.
(32) Bergsma, J. P.; Gertner, B. J.; Wilson, K. R.; Hynes, J. T. *J. Chem. Phys.* **1987**, *86*, 1356.
(33) Williams, I. H. *Chem. Phys. Lett.* **1982**, *88*, 462.
(34) Williams, I. H. *THEOCHEM (J. Mol. Struct.)* **1983**, *11*, 275.
(35) Williams, I. H. *THEOCHEM (J. Mol. Struct.)* **1983**, *14*, 105.
(36) Martí, S.; Moliner, V.; Tuñón, I. *J. Chem. Theory Comput.* **2005**, *1*, 1008.
(37) Aranda, J.; Roca, M.; Lopez-Canut, V.; Tuñón, I. *J. Phys. Chem. B* **2010**, *114*, 8467.
(38) Note that the units given for k_{-1} are due to the fact that we are considering the product complex as the reactant for the backward reaction. The free energy barrier associated to the second-order rate constant can be estimated, assuming that separation of the product fragments does not involve any change in free energy (as suggested by Figure 2) and adding the free energy term due to the volume change needed to change to 1 M standard state (-2.8 kcal·mol^{-1}).
(39) Einstein, A. *Ann. Phys.-Berlin* **1905**, *17*, 549.
(40) Freitas, R. A., Jr. Biocompatibility. In *Nanomedicine*; Landes Bioscience: Georgetown, TX, 2003; Vol. *IIA*.
(41) Steinfeld, J. I.; Francisco, J. S.; Hase, W. L. *Chemical Kinetics and Dynamics*; Prentice-Hall: Upper Saddle River, 1999.
(42) Grote, R. F.; Hynes, J. T. *J. Chem. Phys.* **1980**, *73*, 2715.
(43) Gertner, B. J.; Wilson, K. R.; Hynes, J. T. *J. Chem. Phys.* **1989**, *90*, 3537.
(44) Kim, H. J.; Hynes, J. T. *J. Am. Chem. Soc.* **1992**, *114*, 10508.
(45) Moya-Garcia, A. A.; Ruiz-Pernia, J.; Marti, S.; Sanchez-Jimenez, F.; Tuñón, I. *J. Biol. Chem.* **2008**, *283*, 12393.